JOURNAL OF GEOPHYSICAL RESEARCH, VOL. 113, D02306, doi:10.1029/2007JD008683, 2008

Air pollution radiative forcing from specific emissions sectors at 2030

Nadine Unger,[1] Drew T. Shindell,[1] Dorothy M. Koch,[1] and David G. Streets[2]

Received 21 March 2007; revised 5 September 2007; accepted 7 November 2007; published 25 January 2008.

[1] Reduction of short-lived air pollutants can contribute to mitigate global warming in the near-term with ancillary benefits to human health. However, the radiative forcings of short-lived air pollutants depend on the location and source type of the precursor emissions. We apply the Goddard Institute for Space Studies atmospheric composition-climate model to quantify near-future (2030 A1B) global annual mean radiative forcing by ozone (O_3) and sulfate from six emissions sectors in seven geographic regions. At 2030 the net forcings from O_3, sulfate, black and organic carbon, and indirect CH_4 effects for each emission sector are (in mWm^{-2}) biomass burning, +95; domestic, +68; transportation, +67; industry, −131; and power, −224. Biomass burning emissions in East Asia and central and southern Africa, domestic biofuel emissions in East Asia, south Asia, and central and southern Africa, and transportation emissions in Europe and North America have large net positive forcings and are therefore attractive targets to counter global warming. Power and industry emissions from East Asia, south Asia, and north Africa and the Middle East have large net negative forcings. Therefore air quality control measures that affect these regional sectors require offsetting climate measures to avoid a warming impact. Linear relationships exist between O_3 forcing and biomass burning and domestic biofuel CO precursor emissions independent of region with sensitivity of +0.2 mWm^{-2}/TgCO. Similarly, linear relationships exist between sulfate forcing and SO_2 precursor emissions that depend upon region but are independent of sector with sensitivities ranging from −3 to −12 mWm^{-2}/TgS.

Citation: Unger, N., D. T. Shindell, D. M. Koch, and D. G. Streets (2008), Air pollution radiative forcing from specific emissions sectors at 2030, *J. Geophys. Res.*, *113*, D02306, doi:10.1029/2007JD008683.

1. Introduction

[2] Reduction of short-lived radiatively active air pollutants can contribute to prevent dangerous human-made interference with the climate and at the same time improves air quality [*Hansen et al.*, 2000; *Fiore et al.*, 2002; *Shindell et al.*, 2005a; *West et al.*, 2006; *Hansen et al.*, 2007]. Tropospheric ozone (O_3) and sulfate aerosol are short-lived toxic air pollutants tightly coupled through tropospheric photochemistry and similar human-made emissions sources that influence the Earth's radiation budget, but in opposite ways: increases in O_3 lead to global warming whereas increases in sulfate lead to global cooling. Global modeling studies provide estimates of the global mean radiative forcing of tropospheric O_3 and sulfate for the 1750 to present-day change. The O_3 forcing is estimated to lie in the range +0.25 to +0.65 Wm^{-2} with median value of +0.35 Wm^{-2} and the sulfate forcing is estimated to lie in the range −0.21 to −0.96 Wm^{-2} with a median value of −0.41 Wm^{-2} [*Forster et al.*, 2007]. The magnitude of the sulfate indirect effects through the modification of cloud properties is uncertain but likely to be negative in sign [*Penner et al.*, 2006]. To date, most climate change research and assessment has focused on the role of individual species, and the familiar IPCC radiative forcing bar chart attributes climate forcing in that way [*Forster et al.*, 2007]. However, it is individual human activities such as power generation and transportation that drive the radiative forcings and that may be altered as climate mitigation actions. Previous studies of the assessment of O_3 on climate have usually focused on the role of individual precursor species including NO_x, CO and CH_4 [e.g., *Wigley et al.*, 2001; *Berntsen et al.*, 2005; *Naik et al.*, 2005; *Shindell et al.*, 2005a]. Air quality research has more frequently considered individual emissions sectors, but pollutant reduction measures have not been linked with climate change. Indeed, O_3 and sulfate will continue to be controlled primarily through air quality legislation. Many control measures target an entire activity and thus have implications for all precursor emissions from that activity, and via those, on air quality and climate.

[3] The short atmospheric lifetimes and heterogeneous distributions of O_3 and sulfate are challenges to incorporating these radiatively active species into international climate policy instruments [*Rypdal et al.*, 2005; *Shine et al.*, 2005]. For CO_2 and other long-lived greenhouse gases, the resul-

[1]NASA Goddard Institute for Space Studies, Center for Climate Systems Research, Columbia University, New York, New York, USA.
[2]Argonne National Laboratory, Argonne, Illinois, USA.

0148-0227/08/2007JD008683$09.00

tant radiative forcing is not sensitive to the location of the primary emission. In contrast, O_3 and sulfate are secondary pollutants, formed in the atmosphere from the chemical processing of precursor gases emitted from human activities. O_3 is formed during the oxidation of carbon monoxide (CO), methane (CH_4) or nonmethane volatile organic compounds (NMVOCs) in the presence of sunlight and nitrogen oxides (NO_x) via complex nonlinear photochemical processing. Sulfate is formed from the oxidation of sulfur dioxide (SO_2) via two main pathways: in the gas-phase by the hydroxyl radical (OH) or in the aqueous phase by hydrogen peroxide (H_2O_2) or O_3 (globally the H_2O_2 reaction is of much more importance than the O_3 reaction). O_3 is the source gas for OH and therefore, indirectly H_2O_2 and as such the formation of sulfate aerosol is intimately linked to the photochemical processing that leads to O_3 formation through the availability of oxidants [*Bell et al.*, 2005; *Unger et al.*, 2006a]. A key issue is that the rate of O_3 and sulfate production and hence the resultant climate forcing is dependent on the location of the precursor emissions and the emissions source type.

[4] Direct CH_4 emissions originate from different sectors than O_3 precursors (for example, agriculture and waste management). However, CH_4 and O_3 are strongly coupled through tropospheric photochemistry. CH_4 is a major source of background O_3. At the same time, O_3 photolysis is the major source of OH, which controls the CH_4 lifetime. CH_4 has a considerably longer lifetime than O_3, around 9–10 years in the troposphere, and is itself the second most important greenhouse gas forcing with an estimated value of +0.48 Wm^{-2} since the preindustrial [*Forster et al.*, 2007]. O_3 precursor emissions impact CH_4 forcing indirectly through changing the CH_4 lifetime. CO and NMVOC emissions tend to reduce OH levels and thus increase the CH_4 lifetime. NO_x emissions tend to increase OH and thus decrease the CH_4 lifetime. Several studies have quantified the impact of NO_x emissions on the CH_4 forcing and found that, integrated over time, the indirect CH_4 forcing is similar or larger than the short-term ozone forcing, but of opposite sign [*Wild et al.*, 2001; *Naik et al.*, 2005; *Berntsen et al.*, 2005]. These short-lived precursor emissions induced changes in CH_4 will also affect O_3 on the longer timescale of the CH_4 lifetime [*Berntsen et al.*, 2005; *West et al.*, 2007].

[5] We use a global atmospheric composition-climate model that includes the chemical coupling of O_3 and sulfate to quantify the radiative forcing impacts of both species and the indirect CH_4 forcing due to specific emissions sectors and source regions. The goal of the study is to identify specific emissions sectors and regions where actions could be taken that would most effectively mitigate global warming. The near-future atmosphere at 2030 is chosen for the study because this time frame is the most relevant for policy decisions being made today. In a previous study, we projected changes in O_3, sulfate and CH_4 tropospheric composition at 2030 for a broad range of possible futures [*Unger et al.*, 2006b] including A1B and B1 from the IPCC Special Report of Emissions Scenarios [*Nakicenovic et al.*, 2000] and Current Legislation and Maximum Feasible Reduction from the International Institute for Applied Systems Analysis [*Dentener et al.*, 2004]. We select A1B, a middle-of-the-road projection, for further analyses in the present study. In this scenario, there is a regional shift in precursor emissions at 2030 relative to 1995 from Northern Hemisphere midlatitude regions to subtropical latitudes such as the north African coastline and south Asia where insolation is high and both O_3 and sulfate formation efficiencies increase [e.g., *Berntsen et al.*, 2005; *Koch et al.*, 2007a]. Substantial changes are expected in surface distributions of O_3 and sulfate air pollution for an A1B future. Annual mean surface O_3 concentrations increase around 5–10% across North America and Europe (due to global increases in CH_4 emissions) and up to 40–80% over subtropical regions including India and coastal North Africa. Annual mean surface sulfate concentrations decrease by 50–80% across North America and Europe, but increase dramatically over subtropical regions and so-called developing nations by 50–100%. For the A1B future (including the effects of physical climate changes), the global mean radiative forcings of O_3, sulfate and CH_4 for 2030 relative to 1995 are +140 mWm^{-2}, −220 mWm^{-2} and +250 mWm^{-2}, respectively. The net impact of all short-lived pollutants, including carbonaceous aerosols and changes to indirect aerosol effects, for the A1B scenario is to increase the warming from long-lived greenhouse gases by ∼25% at 2030 [*Shindell et al.*, 2007].

[6] Attributing O_3 pollution to specific source regions is becoming a more active area of research [e.g., *Derwent et al.*, 2004; *Sudo and Akimoto*, 2007]; however, no studies have considered future atmospheres. Quantifying the impacts of individual emissions sectors on O_3 radiative forcing is also newly emerging as an important research area [*Berntsen et al.*, 2006; K. Aunan et al., Radiative forcing from household fuel burning in Asia, submitted to *Proceedings of the National Academy of Sciences*, 2007], although many gaps in our understanding remain. Recent studies have examined the impacts of individual emissions sectors and regions on sulfate, black and organic carbon radiative forcings for the present-day [*Koch et al.*, 2007a] and of sectors for the near future [*Koch et al.*, 2007b]. However, these sulfate and carbonaceous aerosol sector analyses did not include: interactive oxidants, the additional radiative influence of O_3 and the indirect CH_4 forcing effects from the sector, or the impacts of sectors from specific regions. Here we extend and compliment the analyses of *Koch et al.* [2007a, 2007b], and investigate the global mean radiative forcings of O_3 and sulfate and indirect CH_4 effects from 6 emissions sectors (industry, transportation, power, domestic biofuel, domestic fossil fuel and biomass burning) in 7 geographic regions in the A1B 2030 atmosphere. The radiative forcings presented are for concentration changes due to the total emissions from economic sectors at 2030.

2. Model Description

[7] We apply the Goddard Institute for Space Studies (GISS) model for Physical Understanding of Composition-Climate Interactions and Impacts (G-PUCCINI) to investigate climate impacts of anthropogenic emissions sectors at 2030 [*Shindell et al.*, 2006]. The model system is composed of the GISS Model III general circulation model (GCM) [*Schmidt et al.*, 2006] with fully interactive chemistry and aerosols (including sulfate, mineral dust, black and organic carbon and sea salt) and runs seamlessly from the surface up

Table 1. Human-Made Annual Trace Gas Emissions by Sector in Present-Day (1995) and Future (2030 A1B) Simulations[a]

Species	Year	Transportation	Biomass Burning	Power	Industry	Domestic Biofuel	Domestic Fossil Fuel	Total
NO_x, TgN/y	1995	12.7	4.2	7.3	6.1	2.0	1.0	33.2
	2030	17.2	3.8	19.0	10.4	2.1	2.1	54.5
CO, TgCO/y	1995	212.3	314.9	1.8	54.0	226.1	37.6	846.6
	2030	269.1	345.5	5.7	114.1	232.4	35.7	1002.4
NMVOCs, TgC/y	1995	35.5	20.5	0.3	52.3	22.7	1.3	132.6
	2030	48.3	20.8	1.0	98.7	23.4	1.4	193.6
SO_2, TgS/y	1995	6.2	1.3	25.5	33.8	1.4	5.4	73.6
	2030	9.4	1.3	37.4	36.9	1.4	4.2	90.6

[a]The percentage contribution of each emission sector to the total emission is shown in Figure 1.

through the lower mesosphere. For the present study, we do not allow the atmospheric composition to feed back to the climate dynamics through the radiation scheme. We use 23 vertical layers (model top in the mesosphere) and 4 × 5 degree horizontal resolution. The model has been designed with a flexibility to switch on all or different combinations of components of the composition to facilitate investigation of individual or collective interactions between the components. We run using coupled gas-phase chemistry and sulfate aerosol modules, switching off other aerosol types, a configuration previously described in the work of *Bell et al.* [2005]. Chemical calculations are performed only in the troposphere in the present version of the model. We use a thermal tropopause defined by the meteorological lapse rate. Stratospheric values of O_3, NO_x and CH_4 are prescribed according to satellite observations with seasonally varying abundances [*Shindell et al.*, 2003] since A1B 2030 projections of stratospheric composition are not presently available.

[8] The model performance with respect to key short-lived tracers has been comprehensively evaluated for O_3, nitrogen species, and reduced carbon species [*Shindell et al.*, 2006], CO [*Shindell et al.*, 2005b] and sulfate aerosol [*Koch et al.*, 2006, 2007a]. Tropospheric O_3 is well simulated, especially in the vicinity of the tropopause, where it has the greatest effect on climate [*Shindell et al.*, 2006]. The tropospheric chemistry version of G-PUCCINI performed well in a recent multimodel intercomparison involving evaluation against ozonesonde climatology, with a root mean square (rms) error value of 6.3 ppbv compared with a range of RMS error values of 4.6 to 17. ppbv [*Stevenson et al.*, 2006]. Comparisons of the vertical profiles of NO_x and nitric acid (HNO_3) show good agreement between the model and observations from a variety of aircraft measurements across many regions [*Shindell et al.*, 2006]. The model's simulation of CO has been compared extensively with both surface and satellite observations [*Shindell et al.*, 2005b]. It shows good agreement in both magnitude and seasonality, suggesting that the model's OH fields are reasonably realistic. Monthly mean correlations against midtropospheric satellite observations from MOPITT (Measurements of Pollution in the Troposphere) were typically in the range of 0.8–0.9. The sulfate model is generally within a factor of 2 of observations using EDGAR emissions [*Koch et al.*, 2007a] but is biased lower with IIASA emissions [*Koch et al.*, 2006] and in remote regions. Including the heterogeneous interaction between dust and sulfur increases sulfate production and improves the sulfate model with IIASA emissions over Europe [*Bauer and Koch*, 2005].

3. Emissions

[9] The IPCC A1B storyline envisages rapid economic growth, low population growth, the rapid introduction of new and more efficient technologies and a balance between fossil fuel and renewable energy sources. The IMAGE integrated assessment model [*IMAGE Team*, 2001] provided relatively complete documentation of future emissions projections, including explicit energy and fuel usage trends over 17 different regions, which allowed [*Streets et al.*, 2004] to estimate consistent regional growth factors for all the relevant precursor emissions. We apply these regional growth factors to the 1995 inventory from the Emissions Database for Global Atmospheric Research (EDGAR3.2) [*Olivier and Berdowski*, 2001] to derive the full spatial distribution of emissions for each source. The emissions are partitioned into 6 human-made sources: transportation, biomass burning, power, industry, domestic biofuel and domestic fossil fuel [*Streets*, 2007]. The transportation sector includes road and off-road land transportation and shipping. Since approximately 90% of biomass burning, including burning of forests, grasslands, and agricultural waste for land clearing and land use change, has been estimated to be due to anthropogenic activities [*Andreae and Merlet*, 2001], we consider this source human-made for the purpose of the present study.

[10] The global annual sectoral emissions for 2030 A1B are presented in Table 1 along with the EDGAR3.2 1995 values for comparison. Emissions generally increase from 1995 to 2030. Figure 1 shows the fractional contribution of each emissions sector to the total anthropogenic emission for each species and year. Transportation is the dominant sector for NO_x emissions in 1995, but power dominates in the future. Industry and transportation emissions of NO_x increase by 70% and 35% respectively, but the fraction of the total emission remains approximately the same. The dominant source sectors for CO are biomass burning, domestic biofuel and transportation in both 1995 and the future. Industry and transportation are the major source sectors for NMVOCs in 1995 and the future atmosphere, with increases of 89% and 36% respectively between 1995 and 2030. SO_2 emissions are dominated by the power and industry sectors, which both increase at 2030 by 47% and

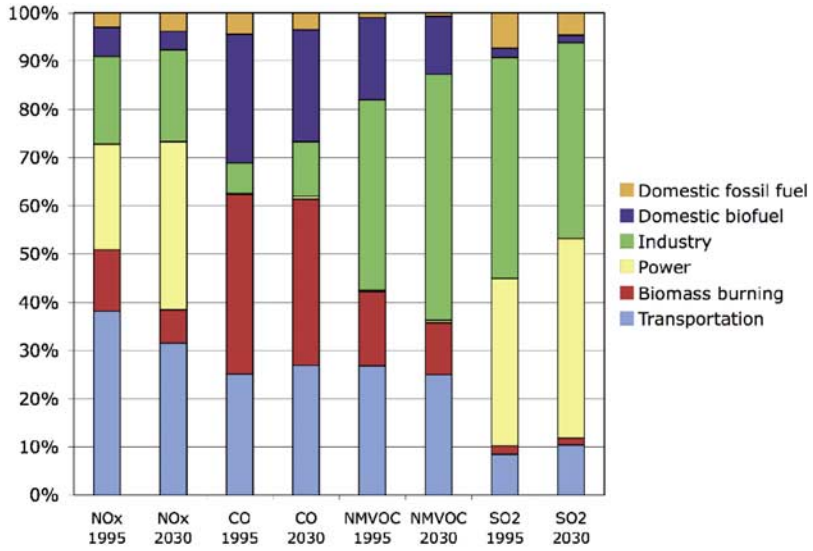

Figure 1. Fractional contribution of each emissions sector to the total emission at 1995 and 2030 for each species (%).

10% respectively relative to 1995. In the present study, CH_4 concentrations are prescribed to values that were generated in previous simulations with the same model but using a fully interactive CH_4 cycle including climate sensitive emissions from wetlands [*Unger et al.*, 2006b]. For the 2030 A1B atmosphere human-made CH_4 emissions increase by 75% relative to 1995, which lead to concentration projections of 2603 ppbv in the Northern Hemisphere and 2353 ppbv in the Southern Hemisphere.

[11] In addition to anthropogenic sources, natural emissions also represent sizable sources of O_3 and sulfate precursors. The natural sources used in the present study are described in more detail in the work of *Unger et al.* [2006b] and include: NO_x from soils (5.8 TgN/y) and lightning (6.2 TgN/y); isoprene from vegetation (550 Tg C/y); NMVOCs from vegetation (30 Tg C/y); SO_2 from volcanoes (10.5 TgS/y); DMS from the oceans (21.2 TgS/y). The emissions of NO_x from lightning and DMS from the ocean are climate sensitive in the present model. Lightning NO_x increases only modestly by 2030 to 6.5 TgN/y while the oceanic DMS emissions increase is negligible (21.3 TgS/y).

4. Simulations

[12] A 2030 control simulation is performed (named 2030C) using the emissions inventory described in the previous section. Prescribed decadal average (2030–2039) sea surface temperatures and sea ice that were generated in a previous simulation of the GISS atmosphere-ocean model provide the lower boundary conditions for the oceans [*Hansen et al.*, 2007]. The future climate simulation is based on long-lived greenhouse gas projections in the A1B scenario consistent with the anthropogenic short-lived trace gas projections and yields an annual global mean surface temperature increase of 0.72°C.

[13] In addition, we perform a large suite of sensitivity experiments based on elimination of individual emission sectors (transportation, biomass burning, power, industry, domestic biofuel and domestic fossil fuel), which we divide into 2 sets. The first set of 6 sensitivity experiments is based on 2030C but with each individual emissions sector in turn completely removed. We also perform a simulation based on 2030C but with all of the 6 human-made emissions sectors removed simultaneously (named 2030C0). In the second set of sensitivity studies, we examine the influence of individual sectors from specific regions. A total of 42 simulations are performed as we selectively eliminate each of 6 emissions sectors in turn from 7 different geographic regions (Europe, North America, South America, south Asia, East Asia, north Africa and the Middle East and central and southern Africa) defined in Figure 2. The regions do not follow strict geopolitical definitions but are chosen to reflect major source areas. CH_4 concentrations for all the sensitivity studies remain at the 2030C control values.

[14] The control and sensitivity simulations are run for 7 years; the first 2 years of the simulations are discarded as spin-up and the remaining 5 years are averaged for analysis. We isolate the radiative forcing contribution due to each emissions sector by taking the difference between the full control 2030C simulation and the relevant sensitivity simulation. The radiative forcings from O_3 and sulfate are calculated as the instantaneous top-of-the-atmosphere (TOA) forcings (long-wave plus short-wave for O_3 and short-wave for sulfate). The resultant short-term O_3 forcing due to the short-lived CO, NO_x and NMVOC precursor emissions from the various sectors is denoted O_3(ST). Due to the large number of sensitivity simulations in the present study, we are not able to determine the stratospheric temperature adjusted radiative forcing. In the case of tropospheric aerosols, the instantaneous forcing is almost identical to the adjusted forcing [*Hansen et al.*, 2005]. For tropospheric O_3, however, the adjusted forcing may be 10–20% less than the instantaneous forcing [*Hansen et al.*, 2005].

[15] In order to determine the indirect CH_4 forcing from the sectors and regions, we first estimate the change in CH_4

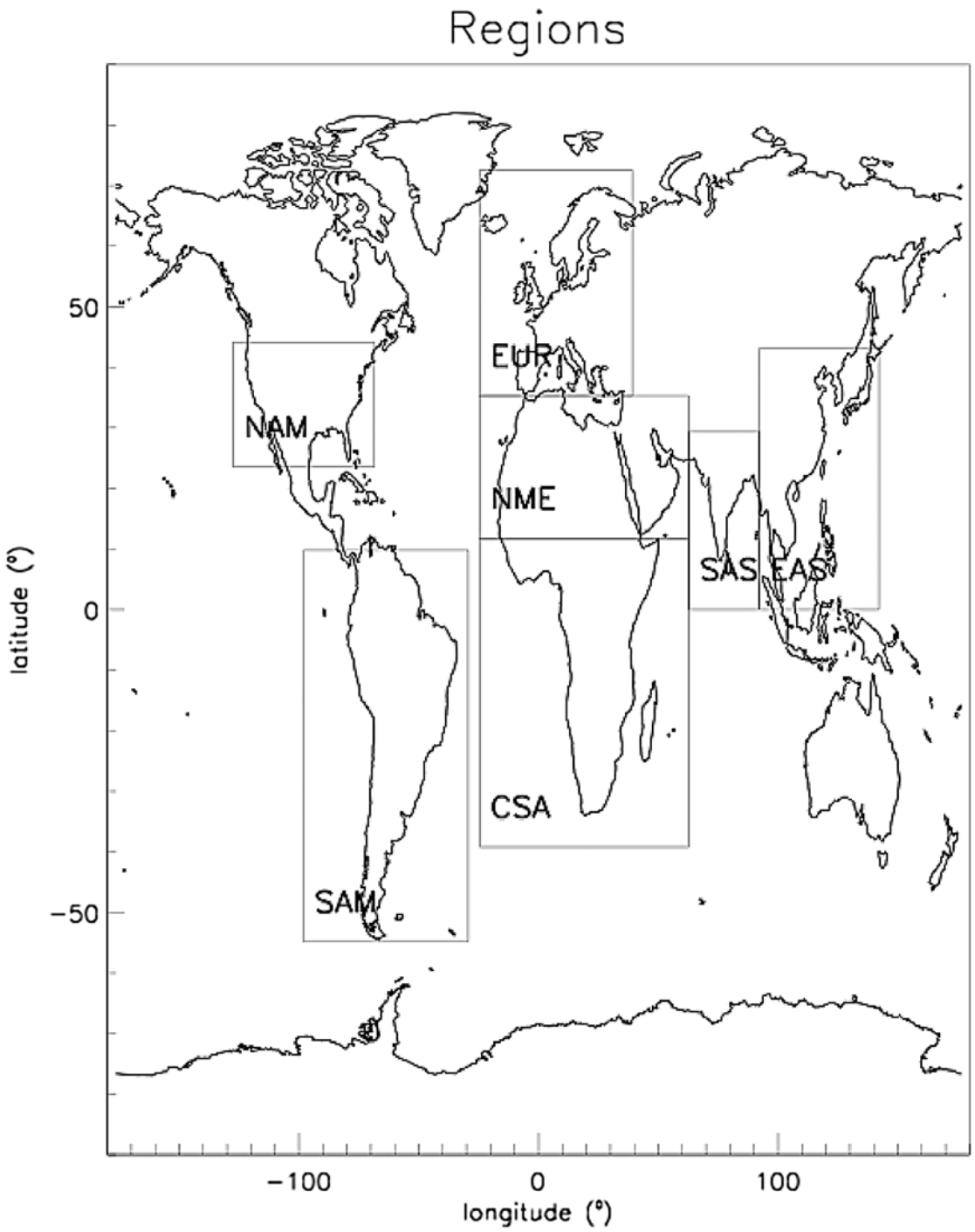

Figure 2. Geographic regions used in the study. Abbreviations are as follows: NAM, North America; EUR, Europe; NME, north Africa and the Middle East; CSA, central and southern Africa; SAS, south Asia; EAS, East Asia; SAM, South America.

concentrations at steady state using the procedure given in the work of *Fuglestvedt et al.* [1999]. The chemical feedback between OH and the CH_4 lifetime is accounted for using a feedback factor of 1.4 [*Prather and Ehhalt*, 2001]. Thus the change in CH_4 at steady state (ΔCH_4) is given by: $\Delta CH_4 = 1.4C_0(\Delta\tau_0/\tau_{ref})$ where C_0 is the initial CH_4 concentration from the control simulation, $\Delta\tau_0$ is the initial change in CH_4 lifetime between the relevant sensitivity and control simulations and τ_{ref} is the CH_4 lifetime in the control simulation. Then, the CH_4 radiative forcing is calculated using a standard simplified expression based on the steady state concentration change [*Ramaswamy et al.*, 2001]. Since CH_4 concentrations are fixed to 2030 values in the sensitivity studies, the effect of the indirect CH_4 changes on the O_3 forcing is estimated using two results from previous multimodel assessment studies: (1) average O_3 response to a 10% enhancement in CH_4 of 0.64 Dobson units [*Gauss et al.*, 2003] (2) average O_3 forcing of

Table 2. Global Annual Mean Radiative Forcing by O_3(ST), O_3(LT) Sulfate, and Indirect Methane (I-CH_4) Owing to Individual Emission Sectors in the 2030 A1B Atmosphere

	ΔRF 2030 A1B, mWm^{-2}				
	O_3(ST)	O_3(LT)	Sulfate	I-CH_4	Net
Transportation	+64	−10	−49	−29	−24
Biomass burning	+50	+7	−12	+19	+64
Power	+37	−17	−197	−49	−226
Industry	+31	−2	−182	−5	−158
Domestic biofuel	+32	+8	−4	+22	+58
Domestic fossil fuel	+6	∼0	−23	+0.1	−17
Sum	+220	−14	−467	−42	−303

0.042 Wm^{-2} per Dobson unit O_3 change [*Ramaswamy et al.*, 2001]. Following the method described in the work of *Berntsen et al.* [2005], we apply these results to the estimated steady state CH_4 concentration changes induced by each emissions sector to determine the associated long-term O_3 forcing that is denoted O_3(LT).

5. Results

5.1. Global Mean Radiative Forcings From Emissions Sectors at 2030

[16] We examine the O_3(ST), sulfate, indirect CH_4 and O_3(LT) radiative forcings in the 2030 A1B atmosphere due to each emissions sector (Table 2). At 2030, the largest O_3(ST) radiative forcings are from the transportation (+64 mWm^{-2}) and biomass burning sectors (+50 mWm^{-2}). The industry, power and domestic biofuel sectors each contribute a similar O_3(ST) forcing, about two thirds to half that of the biomass burning and transportation sectors (∼+35 mWm^{-2}). The largest NO_x source is from the power sector representing 35% of the total emission at 2030. The NO_x source from the biomass burning sector represents only 7% of the total emission at 2030, similar in magnitude to domestic biofuel and domestic fossil fuel sources, but contributes the second largest O_3(ST) forcing response, 35% larger than that from the power sector. The largest sulfate forcings are from the industrial and power sectors (−180 to −190 mWm^{-2}). The transportation sector also contributes a substantial forcing (−49 mWm^{-2}). Biomass burning, domestic biofuel and domestic fossil fuel yield only modest radiative forcings for sulfate (−3 to −20 mWm^{-2}). The sum of the individual emissions sector radiative forcings for O_3(ST) and sulfate are +220 mWm^{-2} and −467 mWm^{-2}, respectively (Table 2). The O_3(ST) and sulfate radiative forcings due to all of the human-made emissions sectors combined (obtained by differencing the 2030C and 2030C0 simulations) are +282 mWm^{-2} and −475 mWm^{-2}. Nonlinearities in the chemistry-climate system mean that combining emissions sectors enhances the radiative forcings of both pollutants compared to the sum of the individual sectors. However, the nonlinear effects are small and 80% of the solution is obtained for O_3(ST) and 98% for sulfate by summing the individual sector contributions.

[17] The indirect impact on CH_4 forcing depends on the photochemical interplay between CO and NO_x from the sector. Sectors with high CO emissions (biomass burning and domestic biofuel) yield positive indirect CH_4 forcings while sectors with high NO_x (power and transportation) yield negative indirect CH_4 forcings. The O_3(LT) forcings mirror the indirect CH_4 forcings but are around one third of the magnitude. The combined indirect CH_4 and O_3(LT) forcing from the power sector (−66 mWm^{-2}) is almost double the O_3(ST) forcing from that sector (+37 mWm^{-2}), but opposite in sign. The transportation sector also contributes negative indirect CH_4 and O_3(LT) forcings, which sum to −39 mWm^{-2}, about two thirds of the magnitude of the O_3(ST) forcing (+64 mWm^{-2}) from that sector. For the domestic biofuel sector, the combined indirect CH_4 and O_3(LT) forcing is almost equal to the O_3(ST) forcing (∼+30 mWm^{-2}) and thus enhances the warming impact of that sector.

[18] Considering the net sum of the O_3(ST), sulfate, indirect CH_4 and O_3(LT) forcings (Table 2), the biomass burning and domestic biofuel sectors have the largest net positive forcings (+64 and +58 mWm^{-2}), while power and industry have large net negative forcings (∼−226 and −158 mWm^{-2}). Transportation and domestic fossil fuel contribute only small net negative forcings (−24 and −17 mWm^{-2}).

[19] We present the air pollutant radiative forcings at 2030 due to individual emissions sectors in Figure 3. Included in Figure 3 for comparison are the sector forcings of black carbon and organic carbon calculated in aerosol-only simulations with the same climate model and discussed in detail elsewhere [*Koch et al.*, 2007b]. The domestic fossil fuel and domestic biofuel sectors are combined into 'domestic' since only that category was available for black and organic carbon. Similar to O_3(ST), the major black carbon positive forcings are form the transportation (+103 mWm^{-2}) and biomass burning (+129 mWm^{-2}) sectors. The largest organic carbon forcing is from biomass burning (−98 mWm^{-2}). Considering the combined net forcing impacts of all the pollutants (shown above each bar in Figure 3), the industrial and power sectors exert an overall negative forcing, whereas biomass burning, transportation and the domestic sectors exert an overall positive forcing indicating that reduction of emissions in these sectors would offer global climate benefits. In particular, the biomass burning sector (net forcing = +95 mWm^{-2}) appears a particularly attractive target to counter global warming.

5.2. Global Mean Radiative Forcings From Emissions Sectors From Specific Regions at 2030

[20] We deepen our investigation by now turning to the impacts of emissions sectors originating from within 7 different regions at 2030. The regions are defined as shown in Figure 2. The annual trace gas emissions from specific regions and sectors are presented in Table 3. EAS provides the largest overall source of each precursor: CO (240 TgCO/y), NO_x (13.9 TgN/y), and SO_2 (32.6 TgS/y). The range of NO_x emitted from the other regions is 7.2 to 4.1 Tg N/y, with EUR at the top end and CSA at the bottom end. The range of SO_2 emitted from the other regions is 9.6 to 4.2 Tg S/y, with SAM at the top end and NAM at the bottom end. The regions have different emissions sector characteristics. In the Northern Hemisphere regions NO_x emissions are dominated by the transportation (∼30–40%), industry (∼20%) and power (∼20–40%) sectors, whereas biomass burning makes large contributions in the Southern Hemisphere regions (∼20–30%). In EUR and NAM, CO emissions are dominated by the transportation sector (∼60%). In the subtropical regions, (EAS, SAS and CSA), the domestic

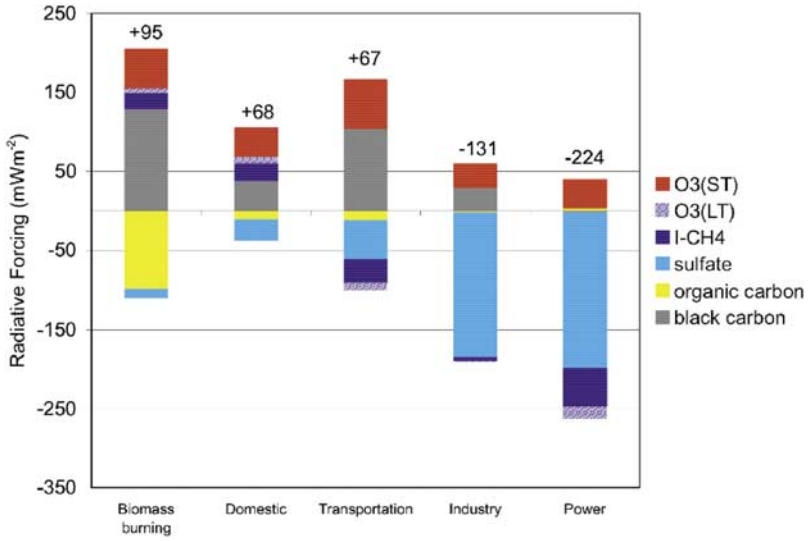

Figure 3. Annual global mean radiative forcing by O_3(ST), sulfate, black carbon, organic carbon, indirect CH_4 (I-CH_4), and O_3(LT) due to individual emission sectors at 2030 in an A1B atmosphere (mWm^{-2}). Black and organic carbon values are from *Koch et al.* [2007b]. Domestic sector includes both biofuel and fossil fuel. The net sum over all components for each sector is shown above each bar.

biofuel sector makes a large contribution to CO emissions (~30–60%). In EAS, CSA and SAM, the biomass burning sector makes a large contribution to the CO emission (~20–60%). However, across all regions, the SO_2 emissions are dominated by the industry and power sectors.

[21] Figure 4 shows the O_3(ST), sulfate, indirect CH_4 and O_3(LT) radiative forcings due to each total emissions sector from each regional emission. The domestic biofuel sector represents a large O_3(ST) forcing for the EAS (+13 mWm^{-2}), SAS (+7 mWm^{-2}) and CSA (+10 mWm^{-2}) regions. Biomass burning represents a large O_3(ST) forcing for the CSA (+15 mWm^{-2}) and SAM (+11 mWm^{-2}) regions. The transportation sector represents an important O_3(ST) forcing for all regions ranging from +5 to +12 mWm^{-2}. The power sector O_3(ST) forcings from EAS (+14 mWm^{-2}) and SAS (+8 mWm^{-2}) are also substantial.

[22] The industry and power sectors dominate the sulfate forcings with largest contributions from EAS, SAS and NME (~−30 to −50 mWm^{-2}). Industry and power SO_2 emissions from NME are only 20% of the value from EAS, but contribute a similar total sulfate forcing, reflecting the different sulfur oxidation capacities between regions [*Koch et al.*, 2007a]. The global mean sulfate forcing is small and positive from NAM and EUR for high CO-emitting sectors (domestic biofuel, transport and biomass burning) owing to coupling between the sulfur and oxidation chemistry. Sulfate loading is increased locally over the source region itself, but the sulfate loading actually decreases in longitu-

Table 3. Human-Made Annual Trace Gas Emissions From Sectors From Regions in the Future Atmosphere (2030 A1B)

Species	Region	Power	Industry	Transport	Domestic Biofuel	Domestic Fossil Fuel	Biomass Burning
NO_x, TgN/y	EUR	2.16	1.57	3.11	0.04	0.30	0.04
	NAM	2.10	1.32	1.79	0.06	0.20	0.17
	EAS	6.19	3.75	2.59	0.64	0.43	0.30
	SAS	2.78	1.00	1.14	0.46	0.08	0.01
	NME	1.28	0.76	3.22	0.04	0.47	0.04
	CSA	0.62	0.23	1.31	0.49	0.17	1.25
	SAM	1.26	0.68	1.40	0.09	0.07	0.84
CO, TgCO/y	EUR	0.77	13.63	38.56	4.40	3.16	4.06
	NAM	1.05	5.36	45.83	6.12	1.15	15.34
	EAS	1.46	35.25	48.29	69.51	20.50	62.29
	SAS	0.52	10.32	12.30	48.43	0.21	1.02
	NME	0.40	15.10	45.86	5.85	1.73	2.52
	CSA	0.13	10.03	20.00	61.50	6.10	89.26
	SAM	0.53	10.79	21.94	7.33	0.25	57.40
SO_2, $TgSO_2$/y	EUR	3.13	2.37	1.04	0.01	0.23	0.01
	NAM	1.85	1.84	0.32	0.01	0.14	0.04
	EAS	15.20	13.88	1.46	0.37	1.49	0.22
	SAS	4.86	2.44	1.29	0.54	0.13	0.01
	NME	2.33	4.30	1.97	0.03	0.79	0.01
	CSA	1.97	2.60	0.79	0.33	0.81	0.43
	SAM	2.37	6.00	0.81	0.01	0.16	0.25

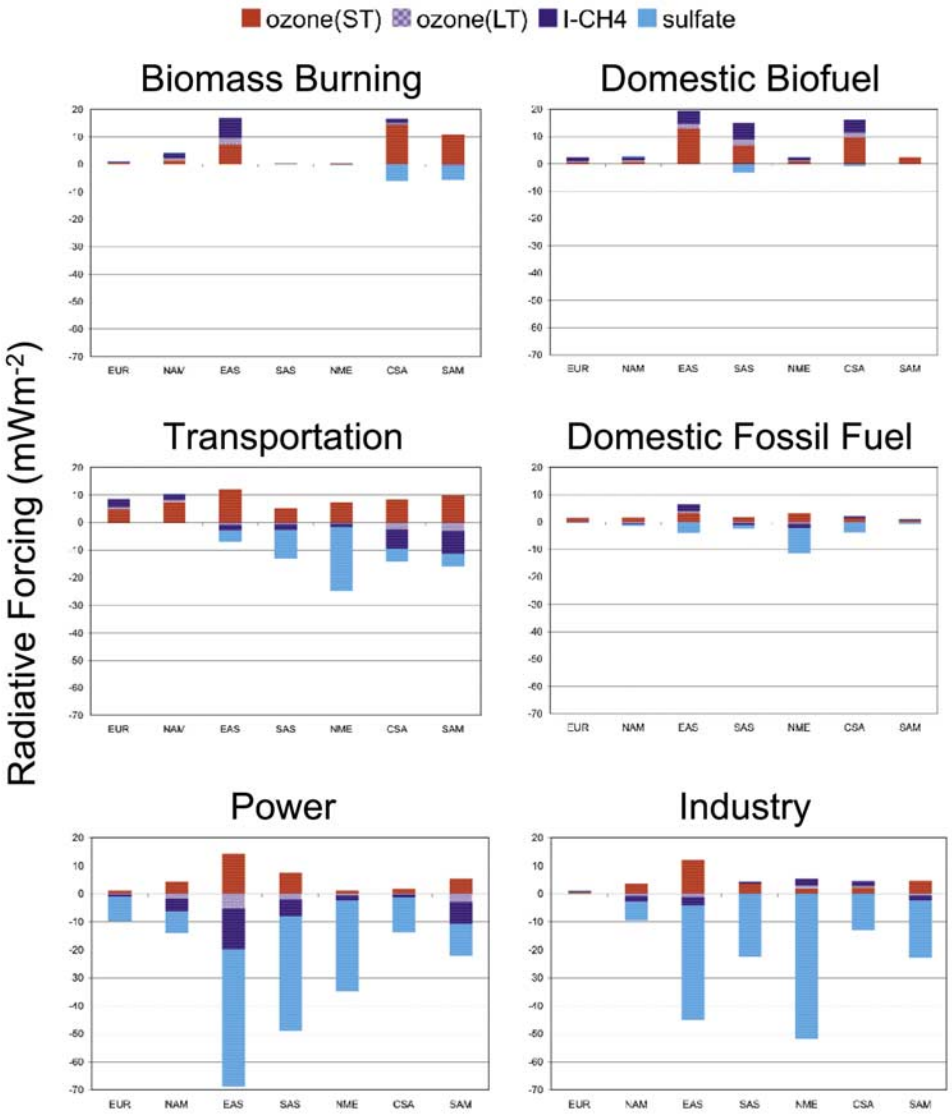

Figure 4. Annual global mean radiative forcing by O_3(ST), sulfate, indirect CH_4 (I-CH_4), and O_3(LT) due to individual emissions sectors from seven regions at 2030 in an A1B atmosphere (mWm^{-2}).

dinal directions away from the region owing to depletion of OH by high CO emissions from those sectors and a corresponding reduction in sulfate formation.

[23] The indirect effects of the sectors from regions on the CH_4 and O_3(LT) forcings are complex. The sign of the indirect CH_4 and O_3(LT) forcings for the transportation, industry and domestic fossil fuel sectors depends on the region. For EUR and NAM, transportation exerts a small positive combined indirect CH_4 and O_3(LT) forcing of around +4 mWm^{-2}. For the Southern Hemisphere regions CSA and SAM, transportation exerts a substantial negative combined indirect CH_4 and O_3(LT) forcing (−10 to −11 mWm^{-2}), exceeding the O_3(ST) forcing but opposite in sign. Substantial positive combined indirect CH_4 and O_3(LT) forcing comes from biomass burning in EAS (+10 mWm^{-2}) and domestic biofuel in EAS (+6 mWm^{-2}), SAS (+8 mWm^{-2}) and CSA (7 mWm^{-2}), which enhances the similar magnitude positive forcing from O_3(ST) in those regional sectors. The power sector in EAS (−20 mWm^{-2}), SAS (−8 mWm^{-2}) and SAM (−11 mWm^{-2}) contributes substantial negative combined indirect CH_4 and O_3(LT) forcing, intensifying the strong cooling influence of sulfate emitted from this sector.

[24] Considering the sum of the O_3(ST), sulfate, indirect CH_4 and O_3(LT) forcings, transportation in EUR and NAM (+10 mWm^{-2}), domestic biofuel in EAS (+20 mWm^{-2}), SAS (+12 mWm^{-2}) and CSA (+16 mWm^{-2}) and biomass burning in EAS (+17 mWm^{-2}) and CSA (+11 mWm^{-2}) appear to be the most attractive targets for climate-motivated emissions reductions. Reduction of all of these regional sectors has the added climate advantage of reducing the CH_4 forcing. The power and industry sectors in EAS, SAS and NME have overall large negative forcings largely owing to sulfate formation. Therefore air quality control measures that affect these regional sectors require offsetting climate measures to avoid a deleterious climate impact. Reduction of emissions from the power sector in EAS,

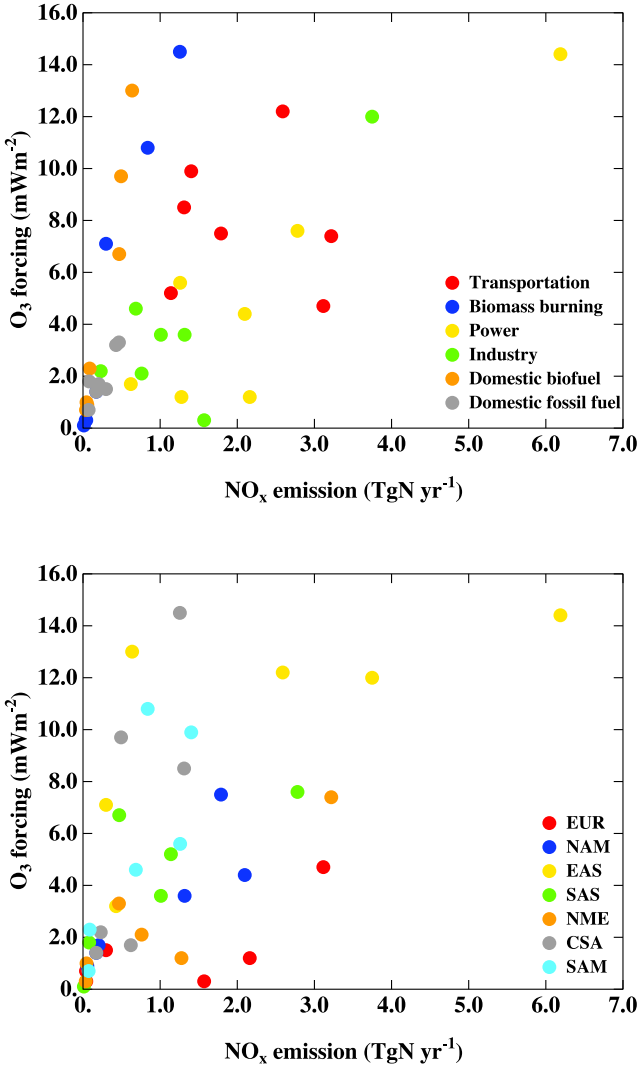

Figure 5a. O_3(ST) radiative forcing response (mWm^{-2}) versus NO_x emission (TgN/y) categorized by (top) emission sector and (bottom) region.

SAS and NME and the industry sector in EAS has the climate disadvantage of increasing the CH_4 forcing.

[25] The relationship between precursor emissions from sectors from regions and the resultant radiative forcings is discussed further in the following section.

5.3. Precursor Emission to Air Pollutant Forcing Diagnostics

[26] We use the data from the 42 sensitivity simulations in the previous section (6 emissions sectors from 7 regions at 2030) and present the global mean O_3(ST) and sulfate radiative forcings as a function of precursor emission mass in Figures 5a–5c. The data are grouped by both emissions sector (top panels) and region (bottom panels). We define a forcing-emission sensitivity factor as the radiative forcing response of a particular air pollutant per unit mass precursor emission. However, since all emissions from a sector and region are removed in the model simultaneously any source coupling will show up as a correlation and thus these derived sensitivities must be used with care. A better approach, beyond the scope of the present study, would be to use numerical sensitivity analysis.

[27] In the case of the O_3(ST) forcing response to NO_x precursor emissions (Figure 5a), no convincing linear correlations are found either by region or sector, highlighting the difficulties in developing effective control strategies for climate-motivated NO_x emissions reduction. However, it is possible to identify different regional sensitivities to NO_x emissions. Global mean O_3(ST) forcings are more sensitive to NO_x emissions from EAS, CSA and SAM than from NAM and EUR (bottom panel of Figure 5a) owing to availability of solar radiation consistent with other studies [*Berntsen et al.*, 2005; *Naik et al.*, 2005].

[28] The global mean O_3(ST) forcing sensitivity to CO emissions is shown by region and sector in Figure 5b. While grouping by region does not provide convincing linear relationship between emission and forcing, very high correlation coefficients for linear regression ($R^2 > 0.95$) are apparent for the high CO-emitting sectors biomass burning and domestic biofuel (top panel of Figure 5b) with forcing-emission sensitivity factors of $0.2 mWm^{-2}$/TgCO. Hence it

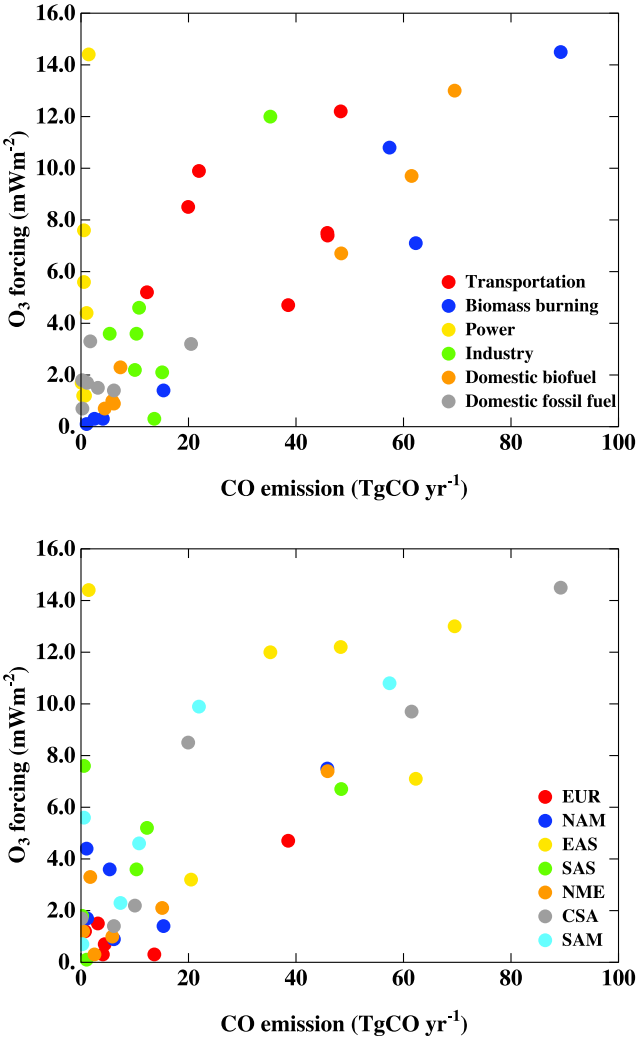

Figure 5b. O_3(ST) radiative forcing response (mWm^{-2}) versus CO emission (TgCO/y) categorized by (top) emission sector and (bottom) region.

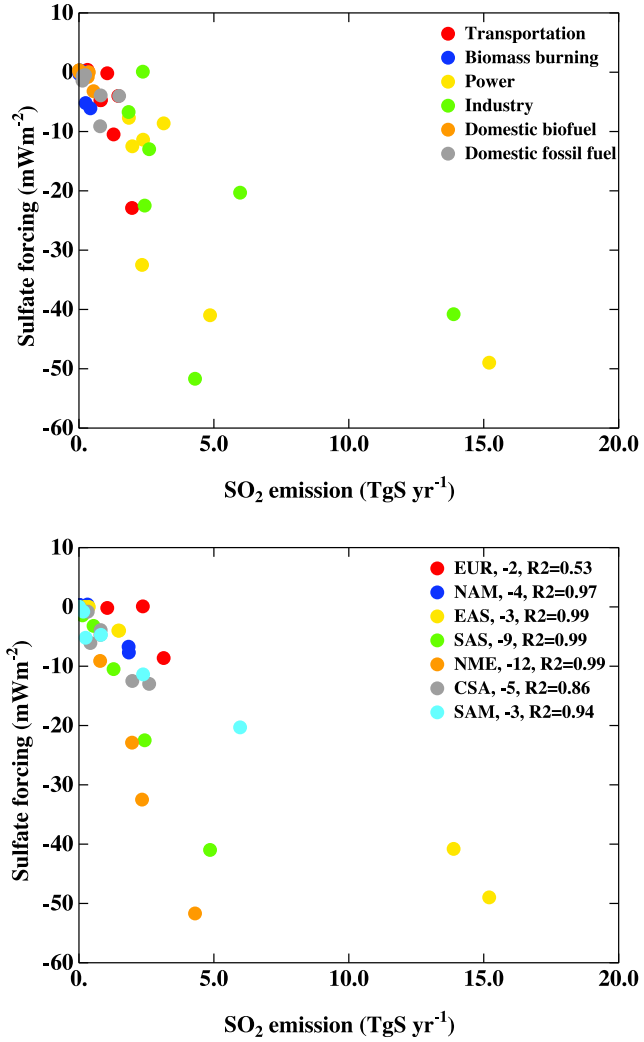

Figure 5c. Sulfate radiative forcing response (mWm^{-2}) versus SO_2 emission (TgS/y) categorized by (top) emission sector and (bottom) region. For the regional analysis the legend includes forcing-emission sensitivity factor, in mWm^{-2}/TgS, and correlation coefficient for linear regression of emissions from different geographic regions.

is possible to relate linearly global mean O_3(ST) forcing to CO precursor emission amount for the high CO-emitting sectors independent of the region of origin in support of *Rypdal et al.* [2005], who advocate the inclusion of CO emissions in the Kyoto Protocol. However, due to nonlinearities in the O_3 formation chemistry, the relationship between O_3(ST) forcing and CO emissions from biomass burning and domestic biofuel result is dependent on the associated NO_x emissions from the sector and the background NO_x field. Further studies would be necessary to ascertain the influence of NO_x on this relationship.

[29] The global mean sulfate forcing is linearly related to SO_2 emissions from regions independent of sector type (bottom panel of Figure 5c). The Figure 5c legend includes forcing-emission sensitivity factors and correlation coefficients for linear regression of global mean sulfate forcing as a function of SO_2 emission by region. The correlation coefficients are all significant ($R^2 > 0.95$), except for EUR and CSA. Forcing-emission sensitivity factors are highest for SAS and NME and lowest for NAM, SAM and EUR as a result of regional differences in available solar radiation, oxidation capacities, wet deposition rates and vertical convective transport rates.

6. Conclusions

[30] We provide new environmental policy-relevant information by quantifying the short-lived air pollutant radiative forcing impacts from specific emissions sectors and regions for the near-future atmosphere, in contrast to providing global-only forcing numbers for each species as in previous studies to date and the IPCC assessments. Such information is essential for the policy analysis community to understand the policy levers available in different sectors and to identify mitigation options that provide the most effective solutions to climate and air quality problems. In order to fully understand the global mean radiative forcings of short-lived pollutants and indirect methane effects from individual emissions sectors and regions, it is necessary to use a global coupled atmospheric composition-climate model. A complex picture emerges when multiple species, sectors and regions are considered.

[31] There are global climate benefits to reducing short-lived air pollutants. At 2030 the net forcings from O_3(ST), sulfate, black carbon, organic carbon, indirect CH_4 and O_3(LT) for each emission sector are (in mWm^{-2}): biomass burning = +95; domestic = +68; transportation = +67; industry = −131; power = −224. Therefore biomass burning emissions are the most attractive target for countering global warming via reduction of air pollution. Reduction of emissions from the transportation sector in Europe and North America and the domestic biofuel sector (especially in East Asia, south Asia and central and southern Africa) would also offer global climate benefits.

[32] Emissions from different sectors and regions have particular characteristics with regard to resultant O_3(ST), sulfate, indirect CH_4 and O_3(LT) global mean forcing impacts. For the total sectors at 2030, biomass burning and domestic biofuel are associated with high O_3(ST) and black carbon forcings and positive indirect CH_4 and O_3(LT) forcings and thus lead to global warming. On the other hand, power and industry sectors are associated with high sulfate and negative indirect CH_4 and O_3(LT) forcings and thus lead to global cooling. Transportation is associated with high O_3(ST) and black carbon, but their positive forcing impact is curbed by the negative indirect CH_4 and O_3(LT) forcings.

[33] Substantial transportation sector O_3(ST) forcings come from all regions (+5 to +12 mWm^{-2}) with Europe and North America appearing to be the most attractive regions for net climate forcing reductions from transportation since the indirect CH_4 and O_3(LT) forcings are also positive from these regions (Figure 4). Additional effects from carbonaceous aerosols are almost exclusively via black carbon (Figure 3), and hence would make emissions reductions even more beneficial toward climate. Central and southern Africa and South America contribute the largest biomass burning O_3(ST) forcings (+11 to +15 mWm^{-2}), comparable to the combined O_3(ST), indirect CH_4 and O_3(LT) forcing from biomass burning in EAS. Domestic

biofuel emissions from East Asia, south Asia and central and southern Africa contribute substantial O_3(ST) forcings (+7 to +15 mWm^{-2}), which are enhanced by positive indirect CH_4 and O_3(LT) forcings ($\sim$+7 mWm^{-2}). The global mean sulfate forcings are dominated by the power and industry sectors with largest contributions from East Asia, south Asia and north Africa and the Middle East (−30 to −50 mWm^{-2}). Moreover, the power sector in East Asia, south Asia and South America also yields negative indirect CH_4 and O_3(LT) forcings (−8 to −20 mWm^{-2}). For the power sector, carbonaceous aerosols are not very important (Figure 3), and hence the forcings from O_3(ST), sulfate, indirect CH_4 and O_3(LT) provide the vast majority of the expected response. This suggests that air quality improvements in East Asia, south Asia, and north Africa and the Middle East could induce substantial global warming, and that measures to improve human health by reducing particulate in these regions should perhaps include climate offsets, and should at minimum be considered in future climate projections.

[34] In order to further inform environmental policy, we identify simple precursor emissions to forcing diagnostics for biomass burning and domestic biofuel CO emissions independent of region (under the associated NO_x conditions), and for SO_2 emissions that depend on region of origin but are independent of emissions sector, which facilitate the inclusion of these short-lived species in policy instruments such as the Kyoto Protocol.

[35] There are some limitations in the present study. The results of the analysis are dependent on the choice of future emissions scenario (A1B) [*Unger et al.*, 2006b]. While all future scenarios project decreases in emissions from domestic fossil fuel, industry and biomass burning sectors, emissions projections from the transportation and power sectors are more variable according to scenario. Indirect aerosol effects are not considered, which represent an additional cooling component to the high sulfate forcing sectors (power and industry) and may alter the net impacts of sectors that emit large amounts of black and organic carbon (transportation and biomass burning). In a semi-quantitative approach, we scale the direct sulfate radiative forcing for the regional sector experiments by the ratio of the indirect forcing (cloud albedo effects) to direct sulfate forcing from the latest IPCC estimate (−0.70 Wm^{-2}/−0.40 Wm^{-2} = 1.75) [*Forster et al.*, 2007]. Inclusion of the aerosol indirect effect via this simple approach results in some changes to regional sectors: the net biomass burning forcing from central and southern Africa would be almost zero and from South America would switch sign to be negative overall (from +5 mWm^{-2} to −4 mWm^{-2}); the net positive domestic biofuel forcing from south Asia would be halved (from +12 to +6 mWm^{-2}); the net transportation forcings from south Asia and north Africa and the Middle East would increase by around a factor of 3 (from −8 and −17 mWm^{-2} to −26 and −57 mWm^{-2}); net negative industry forcings from East Asia and north Africa and the Middle East would increase by around a factor of 3 (from −33 and −46 mWm^{-2} to −104 and −137 mWm^{-2}); net negative power sector forcings from East Asia and south Asia would also exceed −100 mWm^{-2}. Thus indirect aerosol effects may potentially play an important role, but are highly uncertain. Moreover, this simple estimate may exaggerate indirect effects in tropical regions dominated by convective clouds since the GISS model suggests a very small indirect effect for those cloud types [*Menon and Rotstayn*, 2006]. In future work we will include other aerosol types and indirect aerosol effects interactively [e.g., *Menon et al.*, 2002] and investigate the impacts of specific emissions sectors on human health.

[36] In the present study, we consider only short-lived climate forcing agents. The final decision by policy makers about the most effective mitigation options must also include the effects of emissions of long-lived components such as carbon dioxide from each sector and region. Comparison of the climate effects of short- and long-lived climate forcing agents requires the use of advanced metrics such as global warming potential or global temperature change potential [*Fuglestvedt et al.*, 2003; *Shine et al.*, 2007].

[37] **Acknowledgments.** We thank the NASA Atmospheric Chemistry Modeling and Analysis Program (ACMAP) for funding support. We thank the NASA Center for Computational Sciences for computing support.

References

Andreae, M. O., and P. Merlet (2001), Emission of trace gases and aerosols from biomass burning, *Global Biogeochem. Cycles*, *15*, 955–966.

Bauer, S. E., and D. Koch (2005), Impact of heterogeneous sulfate formation at mineral dust surfaces on aerosol loads and radiative forcing in the Goddard Institute for Space Studies general circulation model, *J. Geophys. Res.*, *110*, D17202, doi:10.1029/2005JD005870.

Bell, N., D. Koch, and D. T. Shindell (2005), Impacts of chemistry-aerosol coupling on tropospheric ozone and sulfate simulations in a general circulation model, *J. Geophys. Res.*, *110*, D14305, doi:10.1029/2004JD005538.

Berntsen, T., J. S. Fuglestvedt, M. Joshi, K. P. Shine, N. Stuber, R. Sausen, L. Li, D. A. Hauglustaine, and M. Ponater (2005), Climate response to regional emissions of ozone precursors: Sensitivities and warming potentials, *Tellus, Ser. B*, *57*, 283–304.

Berntsen, T., J. S. Fuglestvedt, G. Myhre, F. Stordal, and T. F. Berglen (2006), Abatement of greenhouse gases: Does location matter?, *Clim. Change*, *74*, 377–411.

Dentener, F., D. Stevenson, J. Cofala, R. Mechler, M. Amann, P. Bergamaschi, F. Raes, and R. Derwent (2004), The impact of air pollutant and methane emission controls on tropospheric ozone and radiative forcing: CTM calculations for the period 1990–2030, *Atmos. Chem. Phys. Disc.*, *4*, 1–68.

Derwent, R. G., D. S. Stevenson, W. J. Collins, and C. E. Johnson (2004), Intercontinental transport and the origins of the ozone observed at surface sites in Europe, *Atmos. Environ.*, *38*, 1891–1901.

Fiore, A. M., D. J. Jacob, B. D. Field, D. G. Streets, S. D. Fernandes, and C. Jang (2002), Linking ozone pollution and climate change: The case for controlling methane, *Geophys. Res. Lett.*, *29*(19), 1919, doi:10.1029/2002GL015601.

Forster, P., et al. (2007), Changes in atmospheric constituents and in radiative forcing, in *Climate Change 2007: The Physical Science Basis*, pp. 131–215, Cambridge Univ. Press, New York.

Fuglestvedt, J. S., T. Berntsen, I. S. A. Isaksen, H. Mao, X.-Z. Liang, and W.-C. Wang (1999), Climatic forcing of nitrogen oxides through changes in tropospheric ozone and methane: Global 3D model studies, *Atmos. Environ.*, *33*, 961–977.

Fuglestvedt, J. S., T. K. Berntsen, O. Godal, R. Sausen, K. P. Shine, and T. Skodvin (2003), Metrics of climate change: Assessing radiative forcing and emission indices, *Clim. Change*, *58*, 267–331, doi:10.1023/A:1023905326842.

Gauss, M., et al. (2003), Radiative forcing in the 21st century due to ozone changes in the troposphere and the lower stratosphere, *J. Geophys. Res.*, *108*(D9), 4292, doi:10.1029/2002JD002624.

Hansen, J., M. Sato, R. Ruedy, A. Lacis, and V. Oinas (2000), Global warming in the twenty-first century: An alternative scenario, *Proc. Natl. Acad. Sci.*, *97*, 9875–9880, doi:10.1073/pnas.170278997.

Hansen, J., et al. (2005), Efficacy of climate forcings, *J. Geophys. Res.*, *110*, D18104, doi:10.1029/2005JD005776.

Hansen, J., et al. (2007), Dangerous human-made interference with climate: A GISS modelE study, *Atmos. Chem. Phys.*, *7*, 2287–2312.

IMAGE Team (2001), *The IMAGE 2.2 Implementation of the SRES Scenarios* [CD-ROM], *Publ. 481508018*, Natl. Inst. for Public Health and the Environ., Bilthoven, Netherlands.

Koch, D., G. A. Schmidt, and C. V. Field (2006), Sulfur, sea salt, and radionuclide aerosols in GISS ModelE, *J. Geophys. Res.*, *111*, D06206, doi:10.1029/2004JD005550.

Koch, D., T. C. Bond, D. Streets, N. Unger, and G. R. van der Werf (2007a), Global impacts of aerosols from particular source regions and sectors, *J. Geophys. Res.*, *112*, D02205, doi:10.1029/2005JD007024.

Koch, D., T. C. Bond, D. Streets, and N. Unger (2007b), Linking future aerosol radiative forcing to shifts in source activities, *Geophys. Res. Lett.*, *34*, L05821, doi:10.1029/2006GL028360.

Menon, S., and L. Rotstayn (2006), The radiative influence of aerosol effects on liquid-phase cumulus and stratiform clouds based on sensitivity studies with two climate models, *Clim. Dyn.*, *27*, 345–356.

Menon, S., A. D. Del Genio, D. Koch, and G. Tselioudis (2002), GCM simulations of the aerosol indirect effect: Sensitivity to cloud parameterization and aerosol burden, *J. Atmos. Sci.*, *59*, 692–713.

Naik, V., D. Mauzerall, L. Horowitz, M. D. Schwarzkopf, V. Ramaswamy, and M. Oppenheimer (2005), Net radiative forcing due to changes in regional emissions of tropospheric ozone precursors, *J. Geophys. Res.*, *110*, D24306, doi:10.1029/2005JD005908.

Nakicenovic, N., et al. (2000), *Special Report on Emission Scenarios*, 559 pp., Cambridge Univ. Press, New York.

Olivier, J. G. J., and J. J. M. Berdowski (2001), Global emissions sources and sinks, in *The Climate System*, edited by J. Berdowski, R. Guicherit, and B. J. Heij, pp. 33–78, A. A. Balkema, Brookfield, Vt.

Penner, J. E., et al. (2006), Model intercomparison of indirect aerosol effects, *Atmos. Chem. Phys. Disc.*, *6*, 1579–1617.

Prather, M., and D. Ehhalt (2001), Atmospheric chemistry and greenhouse gases, in *Climate Change 2001: The Scientific Basis*, edited by J. T. Houghton et al., pp. 239–287, Cambridge Univ. Press, New York.

Ramaswamy, V., et al. (2001), Radiative forcing of climate change, in *Climate Change 2001: The Scientific Basis*, edited by J. T. Houghton et al., pp. 349–416, Cambridge Univ. Press, New York.

Rypdal, K., T. Berntsen, J. S. Fuglestvedt, A. Torvanger, K. Aunan, F. Stordal, and L. P. Nygaard (2005), Tropospheric ozone and aerosols in climate agreements: Scientific and political challenges, *Environ. Sci. Policy*, *8*, 29–43.

Schmidt, G. A., et al. (2006), Present day atmospheric simulations using GISS ModelE: Comparison to in situ, satellite and reanalysis data, *J. Clim.*, *19*, 153–192.

Shindell, D. T., G. Faluvegi, and N. Bell (2003), Preindustrial-to-present-day radiative forcing by tropospheric ozone from improved simulations with the GISS chemistry-climate GCM, *Atmos. Chem. Phys.*, *3*, 1675–1702.

Shindell, D. T., G. Faluvegi, N. Bell, and G. A. Schmidt (2005a), An emissions-based view of climate forcing by methane and tropospheric ozone, *Geophys. Res. Lett.*, *32*, L04803, doi:10.1029/2004GL021900.

Shindell, D. T., G. Faluvegi, and L. K. Emmons (2005b), Inferring carbon monoxide pollution changes from space-based observations, *J. Geophys. Res.*, *110*, D23303, doi:10.1029/2005JD006132.

Shindell, D. T., G. Faluvegi, N. Unger, E. Aguilar, G. A. Schmidt, D. M. Koch, S. E. Bauer, and R. L. Miller (2006), Simulations of preindustrial, present-day, and 2100 conditions in the NASA GISS composition and climate model G-PUCCINI, *Atmos. Chem. Phys.*, *6*, 4427–4459.

Shindell, D. T., G. Faluvegi, S. E. Bauer, D. M. Koch, N. Unger, S. Menon, R. L. Miller, G. A. Schmidt, and D. G. Streets (2007), Climate response to projected changes in short-lived species under the A1B scenario from 2000–2050 in the GISS climate model, *J. Geophys. Res.*, *112*, D20103, doi:10.1029/2007JD008753.

Shine, K. P., T. K. Berntsen, J. S. Fuglestvedt, and R. Sausen (2005), Scientific issues in the design of metrics for inclusion of oxides of nitrogen in global climate agreements, *Proc. Natl. Acad. Sci.*, *102*, 15,768–15,773.

Shine, K. P., T. K. Berntsen, J. S. Fuglestvedt, R. B. Skeie, and N. Stuber (2007), Comparing the climate effect of emissions of short- and long-lived climate agents, *Philos. Trans. R. Soc. Ser. A*, *365*, 1903–1914, doi:10.1098/rsta.2007.2050.

Stevenson, D. S., et al. (2006), Multimodel ensemble simulations of present-day and near-future tropospheric ozone, *J. Geophys. Res.*, *111*, D08301, doi:10.1029/2005JD006338.

Streets, D. G. (2007), Dissecting future aerosol emissions: Warming tendencies and mitigation opportunities, *Clim. Change*, *81*, 313–330, doi:10.1007/s10584-006-9112-8.

Streets, D. G., T. C. Bond, T. Lee, and C. Jang (2004), On the future of carbonaceous aerosol emissions, *J. Geophys. Res.*, *109*, D24212, doi:10.1029/2004JD004902.

Sudo, K., and H. Akimoto (2007), Global source attribution of tropospheric ozone: Long-range transport from various source regions, *J. Geophys. Res.*, *112*, D12302, doi:10.1029/2006JD007992.

Unger, N., D. T. Shindell, D. M. Koch, and D. G. Streets (2006a), Cross influences of ozone and sulfate precursor emissions changes on air quality and climate, *Proc. Natl. Acad. Sci.*, *103*, 4377–4380, doi:10.1073pnas.0508769103.

Unger, N., D. T. Shindell, D. M. Koch, M. Amann, J. Cofala, and D. G. Streets (2006b), Influences of man-made emissions and climate changes on tropospheric ozone, methane, and sulfate at 2030 from a broad range of possible futures, *J. Geophys. Res.*, *111*, D12313, doi:10.1029/2005JD006518.

West, J. J., A. M. Fiore, L. W. Horowitz, and D. L. Mauzerall (2006), Global health benefits of mitigating ozone pollution with methane emission controls, *Proc. Natl. Acad. Sci.*, *103*, 3993–3998.

West, J. J., A. M. Fiore, V. Naik, L. W. Horowitz, M. D. Schwarzkopf, and D. L. Mauzerall (2007), Ozone air quality and radiative forcing consequences of changes in ozone precursor emissions, *Geophys. Res. Lett.*, *34*, L06806, doi:10.1029/2006GL029173.

Wigley, T. M. L., S. J. Smith, and M. J. Prather (2001), Radiative forcing due to reactive gas emissions, *J. Clim.*, *15*, 2690–2696.

Wild, O., M. J. Prather, and H. Akimoto (2001), Indirect long-term global cooling from NO_x emissions, *Geophys. Res. Lett.*, *28*, 1719–1722.

D. M. Koch, D. T. Shindell, and N. Unger, NASA Goddard Institute for Space Studies, Center for Climate Systems Research, Columbia University, 2880 Broadway, New York, NY 10025, USA. (nunger@giss.nasa.gov)

D. G. Streets, Argonne National Laboratory, Argonne, IL 60439, USA.